Electrochimica Acta 419 (2022) 140367

Contents lists available at ScienceDirect

Electrochimica Acta

journal homepage: www.journals.elsevier.com/electrochimica-acta

Stabilizing the high voltage $LiCoPO_4$ cathode *via* Fe-doping in the gram-scale synthesis

Sreekumar Sreedeep [a,1], Subramanian Natarajan [a,1], Yun-Sung Lee [b,*], Vanchiappan Aravindan [a,*]

[a] Department of Chemistry, Indian Institute of Science Education and Research (IISER), Tirupati 517507, India
[b] School of Chemical Engineering, Chonnam National University, Gwang-ju 61186, Republic of Korea

ARTICLE INFO

Keywords:
Cathode
High voltage
Olivine
$LiCoPO_4$
Carbon coating
Low-temperature

ABSTRACT

We report the effect of Fe doping on the electrochemical performance of the olivine structure $LiCoPO_4$. Here, we employed a solid-state approach followed by a carbon coating for the synthesis of $LiFe_xCo_{1-x}PO_4$@C ($0 < x < 0.25$) in a simple two-step procedure. The structural characteristics of the gram-scale prepared cathodes are investigated by various analytical tools and observed that ~10 wt.% of carbon content efficiently enhances the electrical conductivity. The galvanostatic studies endorses an enhancement in the electrochemical performance of $LiFe_xCo_{1-x}PO_4$@C ($0 < x < 0.25$) compared to bare $LiCoPO_4$. Among the various as-synthesized Fe doped samples, $LiFe_{0.1}Co_{0.9}PO_4$@C and $LiFe_{0.15}Co_{0.85}PO_4$@C perform excellent capacity retention characteristics of 67 and 78% after 50 cycles, respectively, and are optimized to be the better Fe dopant concentrations. Further, the cyclic voltammetry and electrochemical impedance spectroscopy studies display better electronic as well as, Li^+ diffusion kinetics upon Fe doping. As a proof of concept, enhancement in Li^+ ion chemical diffusion co-efficient is also observed in the range of 10^{-12} cm^2 s^{-1} in $LiFe_xCo_{1-x}PO_4$@C ($0 < x < 0.25$) whereas only 10^{-15} cm^2 s^{-1} for $LiCoPO_4$. These outcomes recommend this valuable approach toward a gram scale preparation of high voltage Fe-doped $LiCoPO_4$.

1. Introduction

The ever-rising demand of modern society for electric vehicles and hybrid electric vehicles (HEVs) resulted in lots of research towards the development of novel cathode materials for lithium-ion batteries (LIBs). The most commonly employed $LiCoO_2$ cathode has the setbacks of high cost, toxicity, safety issues, and low redox potential triggers the attention to be paid to the cathodes, which can offer several benefits to meet the requirements in electric and hybrid-electric vehicles [1–3]. Cathode materials with olivine structured $LiMPO_4$ (M = Fe, Mn, Co, and Ni) are attractive candidates and possess admirable features of good theoretical capacity (~170 mAh g^{-1}), excellent thermal stability, and high operating voltage [4]. Among these various high-voltage cathodes, $LiFePO_4$ received great attention in this group; however, the low redox potential of $Fe^{2+/3+}$ (3.4 V *vs.* Li) brings a low theoretical energy density of ~580 Wh kg^{-1} as compared to other cathodes. These limitations in $LiFePO_4$ encourage to develop of other members, especially $LiCoPO_4$, owing to its exciting theoretical energy density (800 Wh kg^{-1}), thermal stability originated from the presence of a strong P–O covalent bond of the PO_4^{3-} units, high theoretical capacity (167 mAh g^{-1}), and high redox potential (4.8 V *vs.* Li) of $Co^{2+/3+}$ couple [5–8]. Despite all these desirable properties, the development of $LiCoPO_4$ was hindered by its low electronic conductivity and fast capacity fading. In addition, the higher working potential of the $Co^{2+/3+}$ couple lies beyond the thermodynamic stability window of conventional carbonate electrolytes, leading to electrolyte decomposition, low coulombic efficiency, and robust passivation layer formation [9,10]. This eventually hinders the electrochemical activity of the olivine $LiCoPO_4$ cathodes.

Of the various strategies that are used to improve the electrochemical properties of $LiCoPO_4$, the methods such as carbon coating, ion doping, and electrolyte optimization using additives are gaining lots of interest. Carbon coating aims at improving the electronic conductivity of $LiCoPO_4$, thereby enhancing its reversible Li-insertion/extraction. It was observed that on increasing the amount of added carbon, the electronic

* Corresponding authors.
E-mail addresses: leeys@chonnam.ac.kr (Y.-S. Lee), aravind_van@yahoo.com (V. Aravindan).
[1] These authors contributed equally to this work.

https://doi.org/10.1016/j.electacta.2022.140367
Received 13 October 2021; Received in revised form 7 April 2022; Accepted 8 April 2022
Available online 10 April 2022

conductivity, as well as reversibility, will increase, but beyond a certain limit, both the parameters will decrease [11]. Thus, suggesting the need for an alternate approach that can mitigate the various shortcoming of the carbon coating approach, thereby improving its electrochemical properties. It was further demonstrated the use of ion doping strategy, particularly Fe-doping, in enhancing the bulk electronic conductivity as well as Li^+ ion diffusion rate. Kang et al. [12] observed that this enhanced electrochemical performance up on Fe doping in the Co center of $LiCoPO_4$ was due to suppression of Li–Co anti-site mixing. Along with that, the expansion of the Li^+ ion conduction channel along the [010] direction will also provide evidence for better Li^+ ion conduction. The optimization of the electrolyte using electrolyte additives is another efficient approach that can be used to mitigate the issue of fast capacity fading in $LiCoPO_4$. It was found that the additives will undergo preferential oxidation prior to that of the electrolyte leading to the formation of a protective film over the cathode, thereby preventing the decomposition of electrolyte and also suppressing the side reactions between cathode and electrolyte, thereby mitigating the fast capacity decay in case of $LiCoPO_4$ [13,14].

Taking into account the various setbacks, here we employed a scalable solid-state approach for the synthesis of $LiFe_xCo_{1-x}PO_4$@C ($0 < x < 0.25$), and the structural as well as the electrochemical properties upon Fe doping were also investigated. The improved electrochemical performance of $LiFe_xCo_{1-x}PO_4$@C ($0 < x < 0.25$) occurs due to its enhanced Li^+ ion diffusion as well as electronic conductivity by partial substitution of Co^{2+} and Fe^{2+}, which was one of the major defects associated with $LiCoPO_4$. To further confirm this fact the apparent Li^+ ion diffusion coefficient associated with $LiFe_xCo_{1-x}PO_4$@C ($0 < x < 0.25$) and $LiCoPO_4$ has been determined using the Randles-Sevciks equation.

2. Experimental section

2.1. Synthesis

The $LiFe_xCo_{1-x}PO_4$@C ($0 < x < 0.25$) was prepared by a solid-state synthesis method in a gram scale *i.e.,* 10 gm per batch. In this method, a stochiometric amount of Li_2CO_3 (Sigma-Aldrich, $\geq$ 99%), $(NH_4)_2HPO_4$ (Sigma-Aldrich, $\geq$ 98%), Co_3O_4 (Sigma-Aldrich) and $Fe(CH_3COO)_2$ (Sigma-Aldrich, $\geq$ 99.99%). All the precursors are mixed well and heated to a temperature of 800 °C at a ramp rate of 5 °C min^{-1}. Further, the obtained sample was then ball-milled in a planetary ball-miller (Retsch PM200, Germany) for a duration of 2 h. The ball-milled product was then subjected to the carbon coating, in which glucose (Sigma-Aldrich, $\geq$ 99.5%) was used as the precursor for carbon. Both $LiFe_xCo_{1-x}PO_4$ and glucose were mixed well and made into a solution in a ratio of 2:1 by weight. The solution was then involved in heating so that no more water would remain, and the sample was obtainable in a charred form. The sample was then subjected to heating under an Argon atmosphere to 800 °C at a ramp rate of 5 °C min^{-1}. Finally, the sample was then grounded well into a fine powder using a mortar and pestle.

2.2. Electrolyte preparation

The preparation of electrolyte was done inside an Argon filled Glovebox with an oxygen level of < 0.1 ppm using 1 M $LiPF_6$ dissolved in ethylene carbonate (EC) and dimethyl carbonate (DMC) (1:1 wt ratio, LIPASTE, Tomiyama) along with 10% by volume of fluoroethylene carbonate (FEC) (Sigma-Aldrich, $\geq$ 99.8%) as an additive. None of the solvent or the salt had been subjected to any sort of purification or pretreatment and had been used directly.

2.3. Electrochemical characterization

The half-cell was made in an Argon-filled Glovebox (MBraun, Germany) with an oxygen level of < 0.1 ppm. The electrode was made by mixing 10 mg of $LiFe_xCo_{1-x}PO_4$@C ($0 < x < 0.25$), 2 mg conductive additive (acetylene black) and 2 mg binder (Teflonized acetylene black-2, TAB) in a mortar and pestle using ethanol into a freestanding film. Now the film was then pressed on a 14 mm stainless steel mesh (Goodfellow, UK), which acts as a current collector. The electrode was then kept overnight in a vacuum oven for drying at 75 °C. The electrodes are then inserted into the glove box, and half-cells are made in a CR2016 coin cell with a Glass microfiber separator (Whatman, UK) against metallic Lithium as the counter/reference electrode. The half-cell was made and tested in a battery tester (Biologic, France) for further electrochemical studies. Studies such as electrochemical impedance spectroscopy (EIS, in the range of 10 kHz–1 Hz at an applied a.c. amplitude of 10 mV), galvanostatic charge-discharge, and cyclic voltammetry (CV) were also done for further analysis. In addition, the half-cell performance at different temperatures was carried out in an environmental chamber (Espec, Japan)

2.4. Material characterization

The structural analysis of $LiFe_xCo_{1-x}PO_4$@C ($0 < x < 0.25$) was carried out using X-ray diffraction (XRD, Rigaku, Smart lab 9 kW) at a scan rate of 0.5° min^{-1} in a monochromatic Cu Kα radiation (λ = 1.5414 Å). The Raman spectral analysis was carried out to determine the material composition using a Raman spectrometer (LabRam HR800 UV Raman microscope, Horiba Jobin- Yvon, France).

The surface characterization of the sample was carried out using an X-ray Photoelectron Spectroscopy (XPS, with a multi-lab instrument with a monochromatic Al Kα radiation hν = 1486.6 eV). The internal and morphological analysis of the sample was also carried out using High-resolution transmission electron microscopy (HR-TEM, TECNAI, Philips, the Netherlands, 200 keV) and field emission scanning electron microscopy (FE-SEM, S-4700, Hitachi, Japan). Thermogravimetric analysis (TGA, Shimadzu, Japan) was performed at a ramp rate of 5 °C/min in an air atmosphere.

3. Result and discussion

The structural characterization of $LiFe_xCo_{1-x}PO_4$@C ($0 < x < 0.25$) and $LiCoPO_4$ is as shown (Fig. 1a–h). The XRD-analysis has been carried out to determine the structure as well as phase of $LiFe_xCo_{1-x}PO_4$@C ($0 < x < 0.25$) and $LiCoPO_4$. No characteristic peaks for Fe as well as carbon cannot be observed due to their low content in the sample. But the matching of diffraction peaks of $LiFe_xCo_{1-x}PO_4$@C ($0 < x < 0.25$) and $LiCoPO_4$ suggest the formation of an orthorhombic structure with a *pnma* space group (ICDD No: 89–6192) [5,15]. The Rietveld refinement was done to determine the lattice parameter of the various $LiCoPO_4$ samples, and this can be further used to calculate the unit cell volume and also the crystallite size (Figs. 1b, and S1). Fig. 1b showing the plot of lattice parameters and unit cell volume against different Fe dopant concentrations, depicts that the doping of Fe takes place in the sample, which is attributed to the increase in the unit cell volume as Fe dopant concentration increases as compared to $LiCoPO_4$.The XPS analysis of $LiFe_xCo_{1-x}PO_4$@C was carried out that indicates the presence of elements such as Li, Co, Fe, P, C, and O (Fig. 1c–h). Deconvolution of the Li 1 s, Co 2p, Fe 2p, P 2p, O 1 s, and C 1 s core level will represent the chemical state for each of the elements. Decomposition of C 1 s core level shows peaks positioned at 284.62, 286.59, and 289.63 eV, indicating the presence of C–C, C–OH, and C=O functional groups [16]. The spectrum of Fe exhibits two pairs of peaks corresponding to Fe $P_{1/2}$ and Fe $P_{3/2}$ spin-orbit peaks suggesting the presence of Fe ions in + 2 and + 3 oxidation states on the surface of the prepared composite cathode material. The Co 2p XPS spectra also exhibit two pairs of peaks at ~785 and ~804 eV relates to $CoP_{1/2}$ and $CoP_{3/2}$, respectively, where the satellite peaks further specify the divalent oxidation state of Co ions. The broad peak at 136.5 eV agrees with P $2p_{3/2}$ revealing the oxidation state of P is +5 in PO_4, in agreement with the previous report. Also, there are two peaks observed at ~54.9 eV, conforming to Li^+ and Fe^{2+} in the prepared

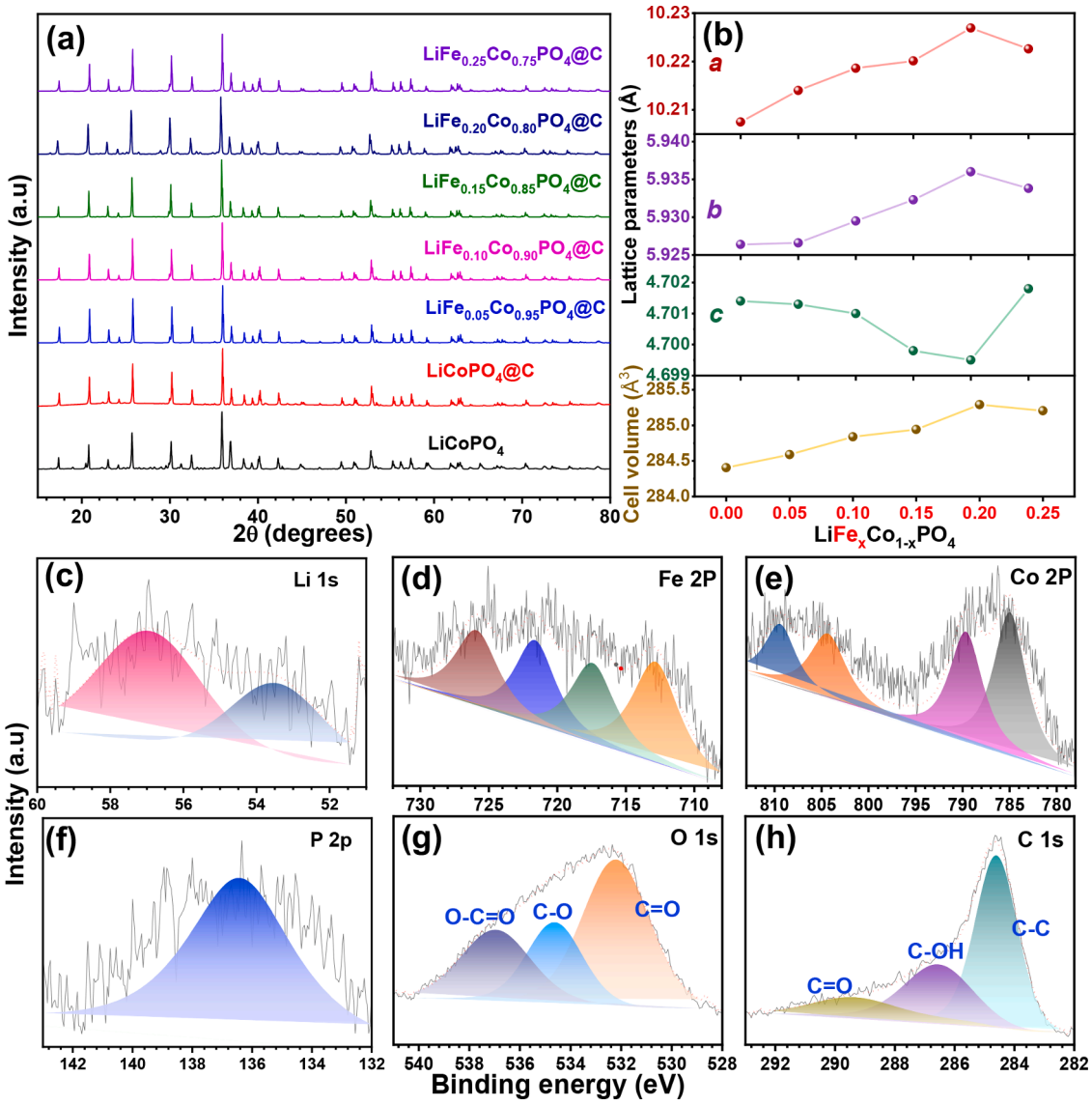

Fig. 1. (a) XRD pattern of $LiFe_xCo_{1-x}PO_4$@C ($0 < x < 0.25$) and $LiCoPO_4$, (b) plot showing the unit cell volume and lattice parameter *vs.* Fe dopant concentration (0–0.25 mol), and (c–h) high-resolution XPS spectra showing the presence of elements Li1s, Fe2p, Co2p, P2p,O1s, and C1s of $LiFe_{0.15}Co_{0.85}PO_4$@C.

cathode material [17]. On decomposing the O1s core level, the peaks are positioned at 532.17, 534.71, and 537.09 eV corresponding to C=O, C–O, and O–C=O modes, respectively. The Raman spectral analysis of $LiFe_{0.15}Co_{0.85}PO_4$@C shows peaks at 1352 and 1603 cm^{-1} corresponding to D-band or defective band and G-band or graphitic band, respectively (Fig. S2). The degree of disorder given by the intensity of D and G bands (I_D/I_G) is calculated to be 0.97, which indicates that the majority of carbons are present in the crystalline state. The amount of carbon content in the sample is determined using TGA analysis and has been found to be ~10 wt.% (Fig. S3). In addition, the strong and prominent peak positioned at 950 cm^{-1} is attributed to be the symmetric stretching mode of the P–O bond in PO_4^{3-} anion. Also, the less intense peak observed at 580 cm^{-1} refers to the Fe dopant [18,19].

The SEM and TEM images of $LiFe_xCo_{1-x}PO_4$@C are shown in Fig. 2. The SEM images (Fig. 2a, b) depict the non-uniform particle size distribution caused by the agglomeration of $LiCoPO_4$ particles during carbon coating. The layer of carbon can also be observed from the TEM image (Fig. 2c, d), which is responsible for the enhanced electronic conductivity. Also, the fringe width has been measured from the TEM image and was found to be 0.389 nm, corresponding to the (1 2 0) plane (Fig. S4). In addition, the SAED pattern (Fig. 2e) also depicts that the compound is highly crystalline. The Energy dispersion X-ray spectroscopy (EDS) (Fig. 2f–j) images indicate the homogenous distribution of elements such as Co, P, O, and Fe in the sample. Thus, all these techniques, including XPS, Raman, SEM, TEM, and EDS analysis, illustrate the formation of $LiFe_xCo_{1-x}PO_4$@C (Fig. S5).

The electrochemical half-cell study for the different Fe dopant compositions is done at a current density of 10 mA g^{-1} between 3.5–5.2 V *vs.* Li. The Fig. 3(a–d) shows the cycling profile of $LiFe_xCo_{1-x}PO_4$@C ($0 < x < 0.25$) and $LiCoPO_4$. From the cycling profile, it can be observed that the discharge capacity, as well as the cycle stability of $LiCoPO_4$, has been enhanced upon Fe doping compared to $LiCoPO_4$. This improved electrochemical performance upon Fe doping occurs due to diminished Li-Co anti-site mixing, which is responsible for the structural stabilization as well as enlarged Li^+ ion transport channel, thereby facilitating Li^+ ion diffusion as well as improved discharge capacity in the case of $LiCoPO_4$ [12,20–23]. Along with Fe doping, the use of FEC as an electrolyte additive also improves the cycle stability by the formation of a stable solid electrolyte interphase (SEI) prior to electrolyte decomposition, thereby preventing the decomposition of electrolyte and also mitigating the side reactions with the electrolyte [15,24,25]. In addition, carbon coating will also enhance the electronic conductivity [11,

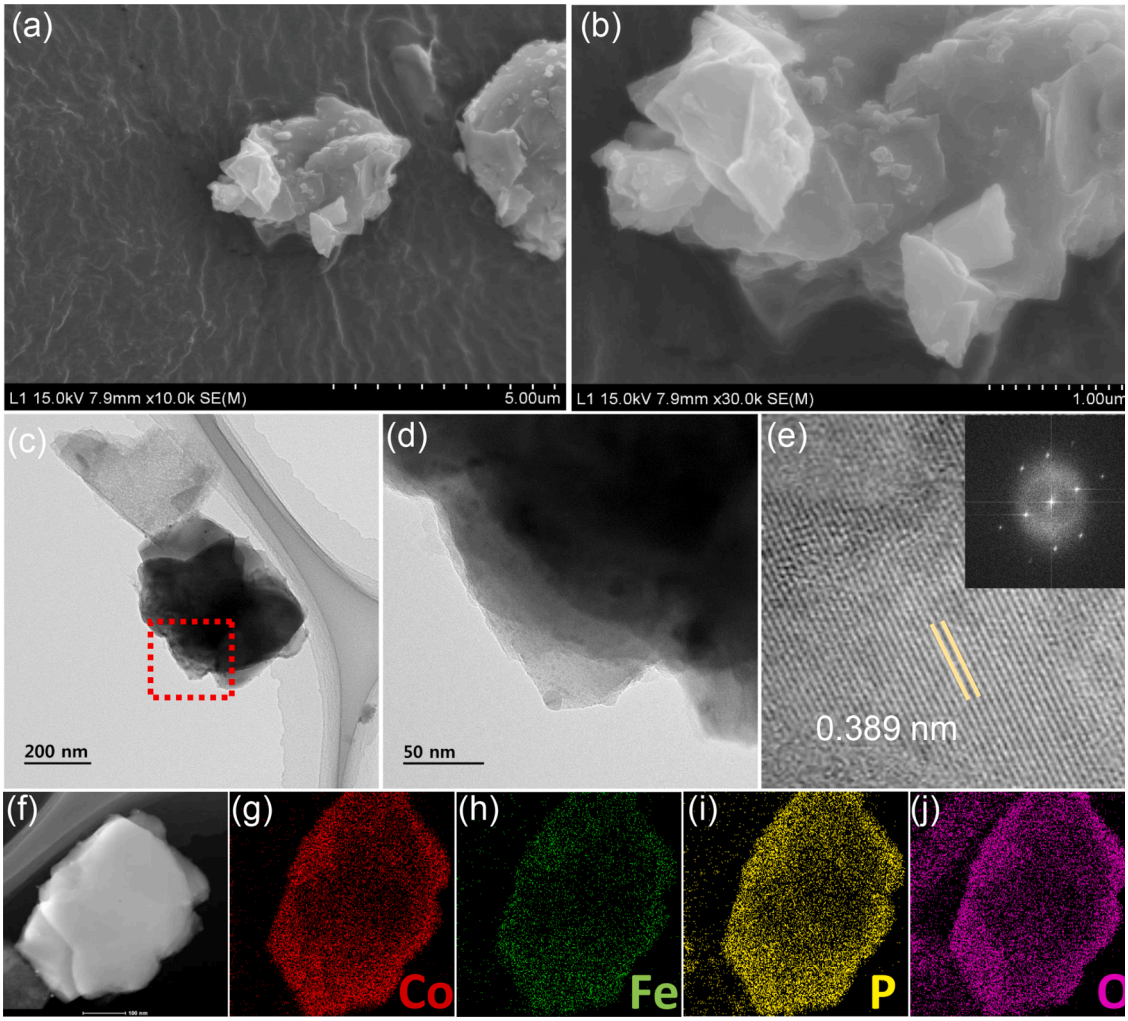

Fig. 2. (a, b) FE-SEM images of $LiFe_{0.15}Co_{0.85}PO_4$@C, (c–e) HR-TEM images of $LiFe_{0.15}Co_{0.85}PO_4$@C, and (f–k) EDS elemental mapping of $LiFe_{0.15}Co_{0.85}PO_4$@C and showing the elemental distribution of Fe, Co, P, and O.

15,25,26]. Thus combined effect of Fe doping, electrolyte additive that is FEC, and carbon coating is responsible for the excellent electrochemical performance of $LiFe_xCo_{1-x}PO_4$@C ($0 < x < 0.25$) compared to $LiCoPO_4$. Now, comparing the electrochemical properties among the different $LiFe_xCo_{1-x}PO_4$@C ($0 < x < 0.25$) cathodes shows that both $LiFe_{0.9}Co_{0.1}PO_4$ and $LiFe_{0.15}Co_{0.85}PO_4$ owing to their high-capacity retention of 67 and 78% and better discharge capacity of 108 and 82 mAh g^{-1}, exhibits better electrochemical performance compared to other Fe dopant concentration. The two plateau voltage peaks observed in the case of $LiCoPO_4$ have a strong dependence on the annealing temperature. A comparison of the charge-discharge curves of $LiCoPO_4$ annealed at low and high temperatures suggests the presence of two-plateau voltage peaks in the case of the former compared to the latter. Here, in the case of $LiFe_xCo_{1-x}PO_4$ ($0 < x < 0.25$), the sample has been annealed at a high temperature of 800 °C for 2 h, which suggests the absence of a two-plateau voltage fingerprint in all the CG voltage plots [27]. In addition, the rate performance plot (Figs. 4a–d, S6a–c) also shows that even at a high current density of 50 mA g^{-1}, the as-prepared $LiFe_{0.15}Co_{0.85}PO_4$ material exhibits maximum capacity retention in comparison to the former $LiFe_{0.1}Co_{0.9}PO_4$@C, which exhibits a mere decrease in capacity retention. At such a high current density, the other doped samples, including $LiFe_{0.05}Co_{0.95}PO_4$@C, $LiFe_{0.2}Co_{0.8}PO_4$@C, and $LiFe_{0.25}Co_{0.75}PO_4$@C, were suffering a fast capacity decay as the current density is increased, which results in low capacity retention. Thus, it can be concluded that the optimum Fe dopant concentration for the better electrochemical performance of $LiFe_xCo_{1-x}PO_4$@C ($0 < x < 0.25$) falls in the range of 0.1–0.15. In addition, the potential *vs.* time plot shown in Fig. S7 exhibit a faster self-discharge in the case of bare $LiCoPO_4$ compared to that of $LiFe_xCo_{1-x}PO_4$@C (*x*: 0.1–0.15), which can be attributed to the low stability of the completely de-lithiated phase of $LiCoPO_4$ compared to that of Fe-doped phase [28]. This clearly indicates the beneficial effect of Fe-doping in the high voltage olivine cathodes. To further study the superior electrochemical performance of $LiFe_{0.9}Co_{0.1}PO_4$ and $LiFe_{0.15}Co_{0.85}PO_4$, a temperature study for the same is also conducted (Fig. 6a, b). From the cycling profile, it can be observed that the electrochemical performance of the samples at low temperatures (–5 and 0 °C) is very poor, while increasing the temperature to 10 and 25 °C, enhancement in the electrochemical performance can be observed. This observation clearly shows that at low temperature, the Li^+ ion mobility will get ceased due to the freezing of the electrolyte solution, which results in large impedance. On the other hand, as the temperature is increased to a moderate value that is 25 °C, the Li^+ ion mobility will get enhanced and thus result in a better electrochemical performance. In addition, from the Nyquist plot (Fig. 5a), a lowering in charge transfer resistance (R_{CT}) can be observed in the case of $LiFe_xCo_{1-x}PO_4$@C ($0 < x < 0.2$), which can be accounted for by the enhanced Li^+ ion diffusion rate upon Fe doping as well as improved electronic conductivity due to carbon coating. But a slight deviation from this trend can be observed with $LiFe_{0.25}Co_{0.75}PO_4$@C, which shows a large R_{CT} even compared to $LiCoPO_4$. This high value of R_{CT} in the case of $LiFe_{0.25}Co_{0.75}PO_4$@C can

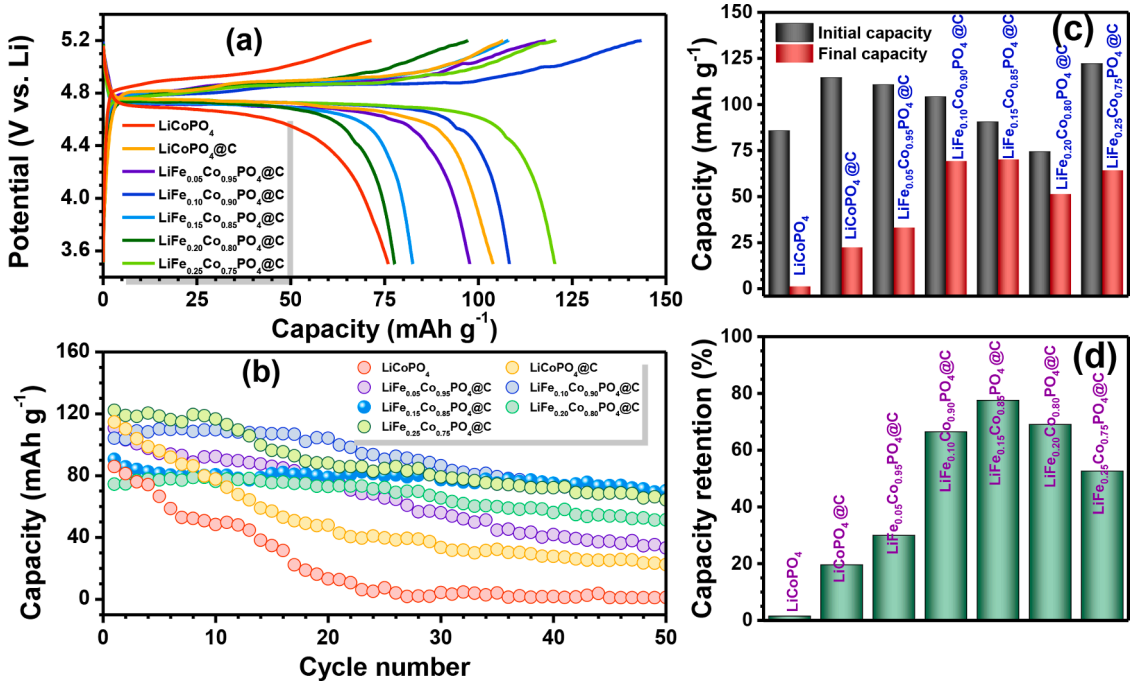

Fig. 3. (a) Charge-discharge curves (b) cycle number *vs.* discharge capacity, (c) initial and final capacity (d) capacity retention of $LiFe_xCo_{1-x}PO_4$@C ($0 < x < 0.25$), and $LiCoPO_4$ at current density of 10 mA g^{-1}, (c).

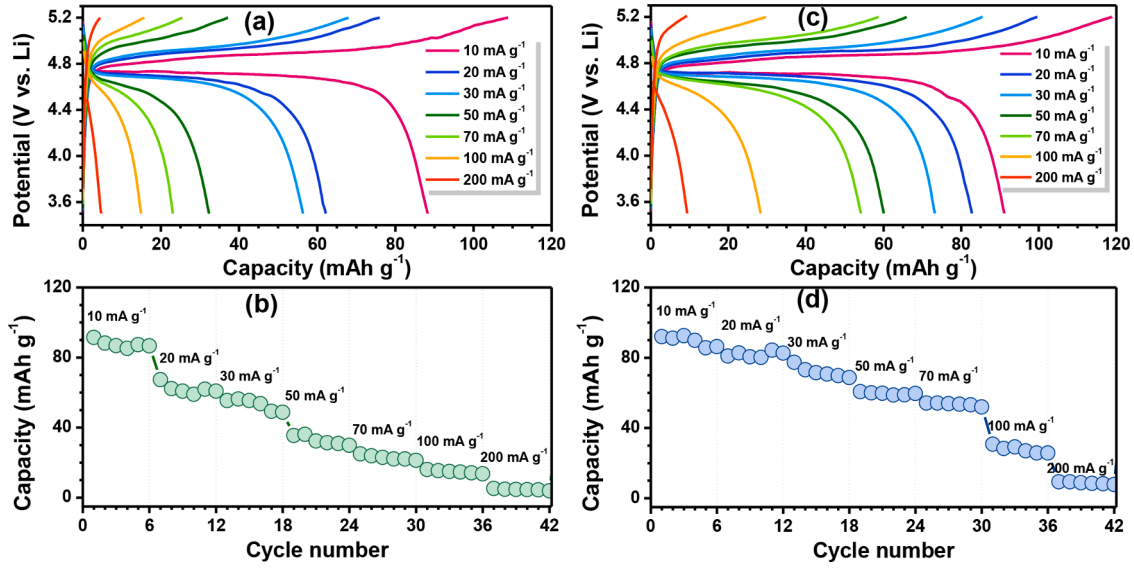

Fig. 4. Rate performance study of (a, b) $LiFe_{0.1}Co_{0.9}PO_4$@C, and (c, d) $LiFe_{0.15}Co_{0.85}PO_4$@C at current densities of 10, 20, 30, 50, 70, 100 and 200 mA g^{-1} between 3.5 and 5.2 V *vs.* Li.

be accounted for by the excess amount of Fe dopant concentration blocking the Li^+ ion conduction. In addition, the low value of R_{CT} for $LiCoPO_4$@C compared to other Fe doped samples is due to the enhanced electronic conductivity upon carbon coating.

To determine the electrochemical reactions occurring during the charge-discharge, the CV of $LiFe_xCo_{1-x}PO_4$@C ($0 < x < 0.25$) and $LiCoPO_4$ is studied at a scan rate of 0.1 mV s^{-1} as shown in Fig. 6a. The different $LiFe_xCo_{1x}PO_4$@C with Fe: 0, 0.05, 0.1, 0.15, 0.2, and 0.25 showed oxidation peaks at 5.07, 5.06, 4.96, 4.98, 5.03, and 4.98 V *vs.* Li, whereas $LiCoPO_4$ shows peaks at 5.11 V *vs.* Li, which is consistent with the charging profile obtained *via* galvanostatic mode. This low charging potential of $LiFe_xCo_{1-x}PO_4$@C compared to $LiCoPO_4$ and $LiCoPO_4$@C can be explained due to oxidation of Fe as well as structural variation occurring during Fe doping in the case of $LiFe_xCo_{1-x}PO_4$@C. Even though a slight displacement in oxidation peak can be observed in the case of Fe doped samples, it can be seen that the reduction peak of $LiCoPO_4$ and $LiFe_xCo_{1-x}PO_4$@C ($0 < x < 0.25$) can be observed at a potential of 4.6 V *vs.* Li.

The apparent Li^+ ion diffusion coefficient for the $LiCoPO_4$ and $LiFe_xCo_{1-x}PO_4$@C ($0 < x < 0.25$) has been evaluated using CV. For the evaluation of diffusion co-efficient, the CVs at various scan rates from 0.1 to 2 mV s^{-1} have been measured. Evaluation of cathodic as well as anodic peak currents has been done against each of the scan rates, and a graph is plotted with peak current (both anodic as well as cathodic) against the square root of the scan rate. The diffusion coefficient for each of the samples was determined using the Randles-Sevcicks equation [12,

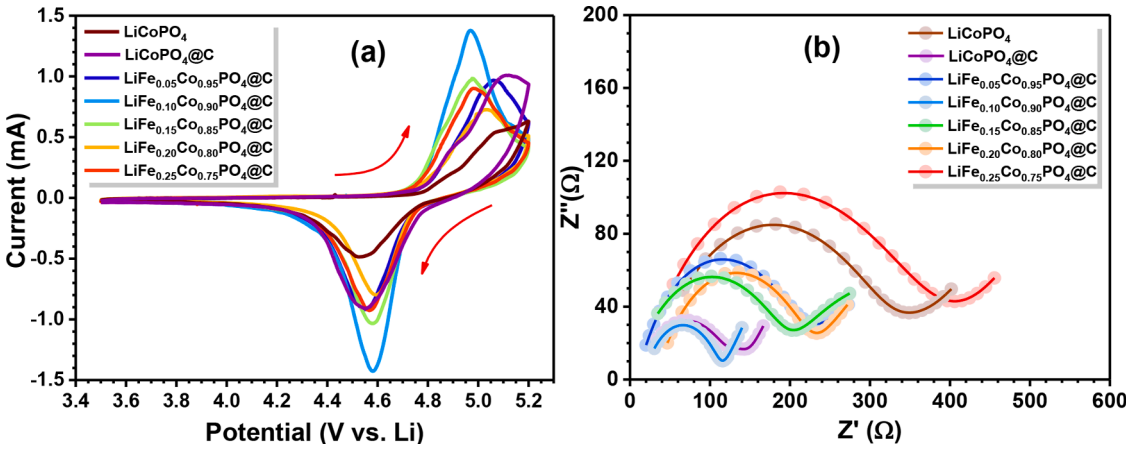

Fig. 5. (a) Cyclic voltammetry curves of $LiFe_xCo_{1-x}PO_4$@C ($0 < x < 0.25$), and $LiCoPO_4$ at a scan rate of 0.1 mV s^{-1}, and (b) Impedance curves of the corresponding samples.

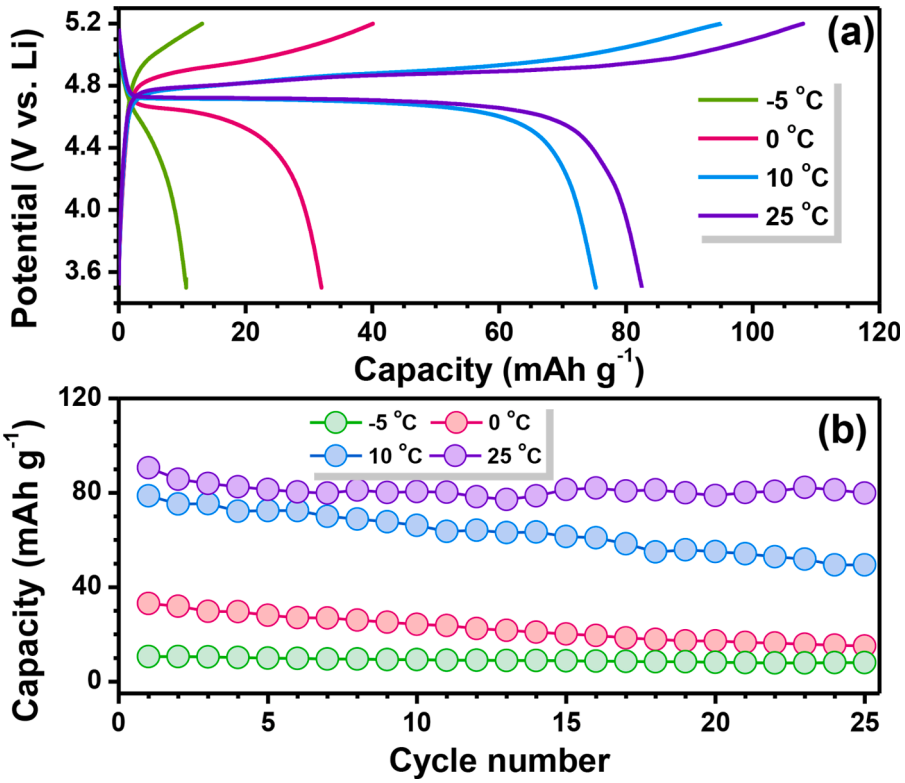

Fig. 6. Temperature-dependent study of $LiFe_{0.15}Co_{0.85}PO_4$@C at a current density of 10 mA g^{-1} (a) charge-discharge curve at different temperatures that is –5, 0, 10, and 25 °C (b) Capacity *vs.* cycle number plot.

21,22,29–31].

$$I_p = 2.69 \times 10^5 n^{3/2} C_0 A\, D^{1/2} v^{1/2}$$

Where I_p is the peak current, n is the number of Li^+ ions, C_0 is the concentration of Li^+ ions, A is the cross-sectional area, D is the diffusion coefficient, and v is the scan rate. Now from the slope of the peak current *vs.* the square root of the scan rate graph (Fig. S8) that is $I_p/v^{1/2}$, the diffusion coefficient can be calculated. Based on the cathodic peak current, it can be observed from Table T1 that the various $LiFe_xCo_{1-x}PO_4$@C ($0.05 < x < 0.25$) show the diffusion coefficient of the order of $\sim 10^{-12}$ cm^2 s^{-1}, which is a much higher compared to $LiCoPO_4$ and $LiCoPO_4$@C, showing the diffusion coefficients of the order of $\sim 10^{-15}$ and $\sim 10^{-14}$ cm^2 s^{-1}. This enhanced value of diffusion coefficient of $LiFe_xCo_{1-x}PO_4$@C ($0.05 < x < 0.25$) compared to $LiCoPO_4$ and $LiCoPO_4$@C is due to widening of diffusion path in case of later compared to former. Thus, the diffusion coefficient evaluation also illustrates the superior electrochemical performance in the case of $LiFe_xCo_{1-x}PO_4$@C ($0.05 < x < 0.25$) compared to the undoped $LiCoPO_4$@C and $LiCoPO_4$ samples.

4. Conclusion

Here, we successfully demonstrated the effect of Fe doping on the electrochemical performance of $LiCoPO_4$. The galvanostatic charge-discharge profile exhibits better electrochemical performance for $LiFe_xCo_{1-x}PO_4$@C ($0 < x < 0.25$) compared to $LiCoPO_4$. In addition, among the different Fe doped samples, the $LiFe_{0.1}Co_{0.9}PO_4$ and

$LiFe_{0.15}Co_{0.85}PO_4$ owing to their better capacity retention of 67 and 78%, were optimized to show better electrochemical performance. The better electronic conductivity, as well as Li^+ ion diffusion, is also exhibited by the CV and EIS analysis. Also, the Li^+ ion diffusion coefficient calculated by the Randles-Sevciks equation is in agreement with the fact that Li^+ ion diffusion will be enhanced upon Fe doping. All these results prove the superior electrochemical performance of $LiFe_xCo_{1-x}PO_4$@C compared to $LiCoPO_4$@C and $LiCoPO_4$. Apart from this, additional works have to be done to extend the work towards realizing the commercial perspective.

CRediT authorship contribution statement

Sreekumar Sreedeep: Conceptualization, Methodology, Validation, Formal analysis, Writing – review & editing. **Subramanian Natarajan:** Validation, Formal analysis, Writing – review & editing. **Yun-Sung Lee:** Writing – review & editing. **Vanchiappan Aravindan:** Conceptualization, Methodology, Validation, Formal analysis, Writing – review & editing.

Declaration of Competing Interest

There are no conflicts to declare.

Acknowledgments

SS acknowledges the Council of Scientific and Industrial Research (CSIR), Govt. of India for the Fellowship. YSL acknowledges the financial support from the National Research Foundation of Korea (NRF) grant funded by the Korean government (Ministry of Science, ICT & Future Planning) (No. 2019R1A4A2001527). VA acknowledges financial support from the Science and Engineering Research Board (SERB), a statutory body of the Department of Science & Technology (DST), Govt. of India, through the Ramanujan Fellowship (SB/S2/RJN-088/2016) and Swarnajayanti Fellowship (SB/SJF/2020-21/12).

Supplementary materials

Supplementary material associated with this article can be found, in the online version, at doi:10.1016/j.electacta.2022.140367.

References

[1] N. Nitta, F. Wu, J.T. Lee, G. Yushin, Li-ion battery materials: present and future, Mater. Today 18 (5) (2015) 252–264, https://doi.org/10.1016/j.mattod.2014.10.040.
[2] J.B. Goodenough, Y. Kim, Challenges for rechargeable Li batteries, Chem. Mater. (2010) 587–603, https://doi.org/10.1021/cm901452z. February 9.
[3] D. Deng, Li-ion batteries: basics, progress, and challenges, Energy Sci. Eng. 3 (5) (2015) 385–418, https://doi.org/10.1002/ese3.95.
[4] A.K. Padhi, K.S. Nanjundaswamy, J.B. Goodenough, Phospho-olivines as Positive-Electrode Materials for Rechargeable Lithium Batteries, J. Electrochem. Soc., 144 (4) (1997) 1188–1194. https://doi.org/10.1149/1.1837571.
[5] M. Zhang, N. Garcia-Araez, A.L. Hector, Understanding and development of olivine $LiCoPO_4$ cathode materials for lithium-ion batteries, J. Mater. Chem. A R. Soc. Chem. (2018) 14483–14517, https://doi.org/10.1039/c8ta04063j.
[6] J. Ludwig, T. Nilges, Recent progress and developments in lithium cobalt phosphate chemistry- syntheses, polymorphism and properties, J. Power Sources 382 (February) (2018) 101–115, https://doi.org/10.1016/j.jpowsour.2018.02.038.
[7] F.C. Strobridge, R.J. Clément, M. Leskes, D.S. Middlemiss, O.J. Borkiewicz, K. M. Wiaderek, K.W. Chapman, P.J. Chupas, C.P. Grey, Identifying the structure of the intermediate, $Li_{2/3}CoPO_4$, formed during electrochemical cycling of $LiCoPO_4$, Chem. Mater. 26 (21) (2014) 6193–6205, https://doi.org/10.1021/cm502680w.
[8] S. Sreedeep, S. Natarajan, V. Aravindan, Recent advancements in $LiCoPO_4$ cathodes using electrolyte additives, Curr. Opin. Electrochem. 31 (2022), 100868, https://doi.org/10.1016/j.coelec.2021.100868.
[9] E. Markevich, R. Sharabi, H. Gottlieb, V. Borgel, K. Fridman, G. Salitra, D. Aurbach, G. Semrau, M.A. Schmidt, N. Schall, et al., Reasons for capacity fading of $LiCoPO_4$ cathodes in $LiPF_6$ containing electrolyte solutions, Electrochem. Commun. 15 (1) (2012) 22–25, https://doi.org/10.1016/j.elecom.2011.11.014.
[10] J. Li, Z. Wang, Triethyl borate and tripropyl borate as electrolyte additives for 4.8V high voltage layered lithium-rich oxide cathode with enhanced self-discharge suppression performance: a comparative study, J. Power Sources 450 (November 2019) (2020), 227648, https://doi.org/10.1016/j.jpowsour.2019.227648.
[11] J. Wolfenstine, J. Read, J.L. Allen, Effect of carbon on the electronic conductivity and discharge capacity $LiCoPO_4$, J. Power Sources 163 (2) (2007) 1070–1073, https://doi.org/10.1016/j.jpowsour.2006.10.010.
[12] Y.M. Kang, Y.I. Kim, M.W. Oh, R.Z. Yin, Y. Lee, D.W. Han, H.S. Kwon, J.H. Kim, G Ramanath, Structurally stabilized olivine lithium phosphate cathodes with enhanced electrochemical properties through Fe doping, Energy Environ. Sci. 4 (12) (2011) 4978–4983, https://doi.org/10.1039/c1ee02283k.
[13] A.M. Haregewoin, A.S. Wotango, B.J. Hwang, Electrolyte additives for lithium ion battery electrodes: progress and perspectives, Energy Environ. Sci. 9 (6) (2016) 1955–1988, https://doi.org/10.1039/c6ee00123h.
[14] L. Yang, T. Markmaitree, B.L. Lucht, Inorganic additives for passivation of high voltage cathode materials, J. Power Sources 196 (4) (2011) 2251–2254, https://doi.org/10.1016/j.jpowsour.2010.09.093.
[15] R. Sharabi, E. Markevich, K. Fridman, G. Gershinsky, G. Salitra, D. Aurbach, G. Semrau, M.A. Schmidt, N. Schall, C. Bruenig, Electrolyte solution for the improved cycling performance of $LiCoPO_4$/C composite cathodes, Electrochem. Commun. 28 (2013) 20–23, https://doi.org/10.1016/j.elecom.2012.12.001.
[16] A. Fujimoto, Y. Yamada, M. Koinuma, S. Sato, Origins of Sp^3C peaks in C_{1s} X-ray photoelectron spectra of carbon materials, Anal. Chem. 88 (12) (2016) 6110–6114, https://doi.org/10.1021/acs.analchem.6b01327.
[17] L. Fang, H. Zhang, Y. Zhang, L. Liu, Y. Wang, Design and synthesis of two-dimensional porous Fe-doped $LiCoPO_4$ nano-plates as improved cathode for lithium ion batteries, J. Power Sources 312 (2016) 101–108, https://doi.org/10.1016/j.jpowsour.2016.02.035.
[18] R. Sharabi, E. Markevich, V. Borgel, G. Salitra, G. Gershinsky, D. Aurbach, G. Semrau, M.A. Schmidt, N. Schall, C. Stinner, Raman study of structural stability of $LiCoPO_4$ cathodes in $LiPF_6$ containing electrolytes, J. Power Sources 203 (2012) 109–114, https://doi.org/10.1016/j.jpowsour.2011.12.018.
[19] X. Wu, M. Meledina, J. Barthel, Z. Liu, H. Tempel, H. Kungl, J. Mayer, R.A. Eichel, Investigation of the Li–Co antisite exchange in Fe-substituted $LiCoPO_4$ cathode for high-voltage lithium ion batteries, Energy Storage Mater. 22 (March) (2019) 138–146, https://doi.org/10.1016/j.ensm.2019.07.004.
[20] D. Di Lecce, J. Manzi, F.M. Vitucci, A. De Bonis, S. Panero, S. Brutti, Effect of the iron doping in $LiCoPO_4$ cathode materials for lithium cells, Electrochim. Acta 185 (2015) 17–27, https://doi.org/10.1016/j.electacta.2015.10.107.
[21] J.L. Allen, T. Thompson, J. Sakamoto, C.R. Becker, T.R. Jow, J. Wolfenstine, Transport properties of $LiCoPO_4$ and Fe-substituted $LiCoPO_4$, J. Power Sources 254 (2014) 204–208. https://doi.org/10.1016/j.jpowsour.2013.12.111.
[22] N.V. Kosova, O.A. Podgornova, E.T. Devyatkina, V.R. Podugolnikov, S.A. Petrov, Effect of Fe^{2+} substitution on the structure and electrochemistry of $LiCoPO_4$ prepared by mechanochemically assisted carbothermal reduction, J. Mater. Chem. A 2 (48) (2014) 20697–20705, https://doi.org/10.1039/c4ta04221b.
[23] J. Wolfenstine, Electrical conductivity of doped $LiCoPO_4$, J. Power Sources 158 (2 SPEC) (2006) 1431–1435, https://doi.org/10.1016/j.jpowsour.2005.10.072. ISS.
[24] N. Ehteshami, L. Ibing, L. Stolz, M. Winter, E. Paillard, Ethylene carbonate-free electrolytes for Li-ion battery: study of the solid electrolyte interphases formed on graphite anodes, J. Power Sources 451 (October 2019) (2020), 227804, https://doi.org/10.1016/j.jpowsour.2020.227804.
[25] Y. Wang, H. Ming, J. Qiu, Z. Yu, M. Li, S. Zhang, Y. Yang, Improving cycling performance of $LiCoPO_4$ cathode material by adding tris(Trimethylsilyl) borate as electrolyte additive, J. Electroanal. Chem. 802 (2017) 8–14, https://doi.org/10.1016/j.jelechem.2017.08.004.
[26] Gangulibabu, K. Nallathamby, D. Meyrick, M. Minakshi, Carbonate anion controlled growth of $LiCoPO_4$/C nanorods and its improved electrochemical behavior, Electrochim. Acta 101 (2013) 18–26, https://doi.org/10.1016/j.electacta.2012.09.115.
[27] N.N. Bramnik, K.G. Bramnik, T. Buhrmester, C. Baehtz, H. Ehrenberg, H. Fuess, Electrochemical and structural study of $LiCoPO_4$-based electrodes, J. Solid State Electrochem. 8 (8) (2004) 558–564, https://doi.org/10.1007/s10008-004-0497-x.
[28] J. Manzi, F.M. Vitucci, A. Paolone, F. Trequattrini, D. Di Lecce, S. Panero, S. Brutti, Analysis of the self-discharge process in $LiCoPO_4$ electrodes: bulks, Electrochim. Acta 179 (2015) 604–610, https://doi.org/10.1016/j.electacta.2015.03.071.
[29] X. Wu, M. Meledina, H. Tempel, H. Kungl, J. Mayer, R. Eichel, Morphology-controllable synthesis of $LiCoPO_4$ and its influence on electrochemical performance for high-voltage lithium ion batteries, J. Power Sources 450 (October 2019) (2020), 227726, https://doi.org/10.1016/j.jpowsour.2020.227726.
[30] W.F. Howard, R.M. Spotnitz, Theoretical evaluation of high-energy lithium metal phosphate cathode materials in Li-ion batteries, J. Power Sources 165 (2) (2007) 887–891, https://doi.org/10.1016/j.jpowsour.2006.12.046.
[31] S. Brutti, J. Manzi, D. Meggiolaro, F.M. Vitucci, F. Trequattrini, A. Paolone, O. Palumbo, Interplay between local structure and transport properties in iron-doped $LiCoPO_4$ olivines, J. Mater. Chem. A 5 (27) (2017) 14020–14030, https://doi.org/10.1039/c7ta03161k.